Journal of Applied Physics

Direct observations of crystallization processes of amorphous GeSn during thermal annealing: A temperature window for suppressing Sn segregation

Cite as: J. Appl. Phys. **125**, 175703 (2019); https://doi.org/10.1063/1.5086480
Submitted: 21 December 2018 . Accepted: 13 April 2019 . Published Online: 02 May 2019

Masashi Higashiyama, Manabu Ishimaru, Masayuki Okugawa, and Ryusuke Nakamura

Journal of Applied Physics ARTICLE scitation.org/journal/jap

Direct observations of crystallization processes of amorphous GeSn during thermal annealing: A temperature window for suppressing Sn segregation

Cite as: J. Appl. Phys. **125**, 175703 (2019); doi: 10.1063/1.5086480
Submitted: 21 December 2018 · Accepted: 13 April 2019 ·
Published Online: 2 May 2019

Masashi Higashiyama,[1] Manabu Ishimaru,[1,a)] Masayuki Okugawa,[2] and Ryusuke Nakamura[2]

AFFILIATIONS

[1]Department of Materials Science and Engineering, Kyushu Institute of Technology, Kitakyushu, Fukuoka 804-8550, Japan
[2]Department of Materials Science, Osaka Prefecture University, Sakai, Osaka 599-8531, Japan

[a)]**Author to whom correspondence should be addressed:** ishimaru@post.matsc.kyutech.ac.jp

ABSTRACT

The solubility limit of tin (Sn) in germanium (Ge) is very small, and, therefore, it is difficult to synthesize high Sn concentration GeSn crystals by conventional methods. An amorphous phase can contain elements beyond the solubility limit of the crystal state, and, therefore, recrystallization of the amorphous alloy is one of the possible ways to realize materials far from the equilibrium state. To suppress Sn precipitation during thermal annealing, knowledge of crystallization processes is required. In the present study, amorphous GeSn thin films with different Sn concentrations were prepared by sputtering, and their crystallization processes were examined by *in situ* transmission electron microscopy. It was found that the crystallization temperature decreases with increasing Sn concentration, and it became lower than the eutectic temperature when the Sn concentration exceeded ~25 at. %. Radial distribution function analyses revealed that phase decomposition occurs in the amorphous state of the specimens which crystallize below the eutectic temperature, and Sn crystallites were simultaneously precipitated with crystallization. On the other hand, no remarkable phase decomposition was detected in amorphous GeSn with <25 at. % Sn. Sn precipitation occurred at a higher temperature than the crystallization in these specimens, and the difference between the crystallization and Sn precipitation temperatures became large with decreasing Sn concentration. Because of the existence of this temperature difference, a temperature window for suppressing Sn segregation existed. We demonstrated that large GeSn grains with high Sn concentration could be realized by annealing the specimens within the temperature window.

I. INTRODUCTION

Since germanium-tin (GeSn) possesses higher carrier mobilities than Si and Ge, it is anticipated as a channel material for high performance thin film transistors.[1,2] In addition, its electronic band structure changes from an indirect to direct gap at 6–10 at. % Sn,[3–5] which is useful for optoelectronic applications and high efficiency solar cells. For these applications, it is necessary to control Sn concentration over a wide range. However, the low solubility limit of Sn in Ge (~1 at. % Sn)[6] gives rise to a phase decomposition of crystalline GeSn during heat treatments, and, therefore, much effort has been devoted to overcome this obstacle. Chemical vapor deposition and molecular beam epitaxy can directly fabricate single crystalline GeSn thin films with high Sn concentration on substrates and have successfully grown crystalline films of high Sn concentration, up to 20%, in thicknesses of up to 500 nm.[7,8]

Another approach to realize atomic arrangements and microstructures far from the equilibrium state is to utilize recrystallization from an amorphous phase, which is easier and cheaper than chemical vapor deposition and molecular beam epitaxy. In fact, this procedure has already been applied to commercial production. For example, Fe-based soft magnetic alloys consisting of very uniform nanocrystallites with a size of ~10 nm, so-called FINEMET®, were fabricated by the recrystallization of amorphous ribbons.[9] Indeed, some researchers have succeeded in fabricating GeSn with high Sn concentration beyond the solubility limit by recrystallizing amorphous GeSn.[10–15] Also, several researchers tried to increase the grain

size of crystallites,[10,13,16,17] in order to improve the performance of GeSn as a thin film transistor or solar cell. To realize large GeSn grains with a high Sn concentration, knowledge of amorphous structures of GeSn and their crystallization processes is required.

A transmission electron microscope (TEM) equipped with a heating holder is useful for directly observing the structural changes during heat treatments.[15,18] In addition, atomic pair-distribution functions characterizing short-range order of amorphous structures can be obtained by a quantitative analysis of electron diffraction intensities.[19–23] Because of the short wavelength of high-energy electrons, an intensity profile up to high scattering angles is easily obtained by electron diffraction techniques. This is helpful for distinguishing the atomic pairs with slightly different atomic distances from one another.[18,20,21,24] In the present study, we examined the amorphous structures of GeSn and their crystallization processes using *in situ* TEM.

II. EXPERIMENTAL PROCEDURES

Amorphous GeSn thin films with a thickness of 40 nm were prepared by radio frequency magnetron sputtering at a base pressure of 3×10^{-5} Pa. Thin films with reproducible composition can be fabricated by using sintered target materials. However, a Ge target along with square Sn chips was used in the present study, because it is easier to change Sn concentration by controlling the number of chips and is cheaper than the sintered target. The GeSn thin films were deposited on a cleaved NaCl substrate at ambient temperature. The film and substrate were placed in distilled water, and then the floating film was recovered on a molybdenum grid for TEM observations. The specimens were observed by a JEOL JEM-3000F (operated at 300 kV). The Sn concentration of the as-sputtered GeSn was estimated by a quantitative analysis of energy-dispersive x-ray spectroscopy. The spectra were taken from several different areas of a TEM specimen, and it was confirmed that the Sn concentration is almost the same. This suggests that the specimens obtained here are homogeneous.

To examine the thermally-induced structural changes, the specimens were annealed in a TEM using a heating holder. Table I summarizes the specimens, annealing conditions, and research purpose. Electron diffraction patterns were recorded on an imaging plate (Eu^{2+}-doped BaFBr) which has higher sensitivity, wider dynamic range, and better linearity for electron-beam intensities compared with the commercial TEM film material. To evaluate short-range order of

TABLE I. Summary of the specimens used in the present study. Sn concentration is that of the as-sputtered amorphous GeSn measured by energy-dispersive x-ray spectroscopy.

Sample #	Sn concentration (at. %)	Annealing condition	Purpose
1	9.1	No annealing	Structural analysis of the as-sputtered amorphous GeSn (Figs. 1 and 2)
2	16.4		
3	23.9		
4	39.6		
5	20.8	Repeatedly annealed between RT and elevated temperature	Thermally-induced structural changes of amorphous GeSn (Fig. 3)
6	30.3		
7	20.8	Annealed at elevated temperature and then cooled to RT	Confirmation of Sn segregation by thermal annealing (Fig. 4)
8	40.9		
9	21.7	Successive annealing to confirm crystallization and grain growth	Observation on structural evolution with increasing annealing temperature (Fig. 5)
10	9.1	Successive annealing up to crystallization	Estimation of crystallization and Sn segregation temperatures (Fig. 6)
11	11.6	+	
12	16.4	Repeatedly annealed between RT and elevated temperature after crystallization	
13	20.1		
14	21.7		
15	23.9		
16	30.3		
17	39.6		
18	40.9		
19	11.6	Repeatedly annealed between RT and elevated temperature	Changes of lattice parameter and Sn concentration during thermal annealing (Fig. 7)
20	20.1		
21	25.4		
22	39.6		
23	12.0	Annealing at a temperature window	Grain growth without Sn precipitation (Figs. 8 and 9)
24	6.3		

amorphous structures, atomic pair-distribution functions were obtained by a quantitative analysis of electron diffraction intensities. The detailed procedures for the structural analysis have been described elsewhere.[22]

III. RESULTS AND DISCUSSION

A. Amorphous structures of as-sputtered GeSn as a function of Sn concentration

As we reported previously,[25,26] the as-sputtered specimens possessed an amorphous structure with the Sn concentration ranging from ~10 to ~40 at. %. No Sn precipitation was detected, though the Sn concentration is much larger than the solubility limit of Sn in crystalline Ge. Figure 1 shows selected-area electron diffraction patterns obtained from amorphous GeSn with (a) 9.1 and (b) 39.6 at. % Sn. It is apparent that the diameter of the second halo ring in Fig. 1(a) is larger than that in Fig. 1(b), suggesting that the amorphous structure is different between these specimens. To obtain the information of the amorphous structure, we performed a quantitative analysis of electron diffraction intensities. Figure 1(c) shows reduced interference functions, F(Q), of the as-sputtered specimens as a function of Sn concentration. The Sn concentration of the as-sputtered amorphous GeSn was estimated by energy-dispersive x-ray spectroscopy. The scattering vector in reciprocal lattice space is defined as $Q = 4\pi \sin\theta/\lambda$, where θ and λ are the scattering half-angle and the electron wavelength, respectively. For the specimens with 9.1 and 16.4 at. % Sn, a very weak amplitude is recorded up to high scattering angles as high as $Q \sim 320\ nm^{-1}$, well above the background intensity level of the imaging plate. On the other hand, the amplitude at the higher-scattering angle becomes small with increasing Sn concentration. It is empirically known that the diffraction intensities of metallic glasses rapidly damp with increasing scattering angle.[27–29] Based on this knowledge, we speculate that Sn atoms form covalent bonds at low concentrations, while the metallic bonds become important at high Sn concentrations. The wavelength of the F(Q) becomes short with increasing Sn concentration, suggesting an increase of the average bond length at the first nearest neighbor.

Figure 2(a) shows atomic pair-distribution functions, g(r), calculated by Fourier transforming the F(Q) of Fig. 1(c). The g(r)

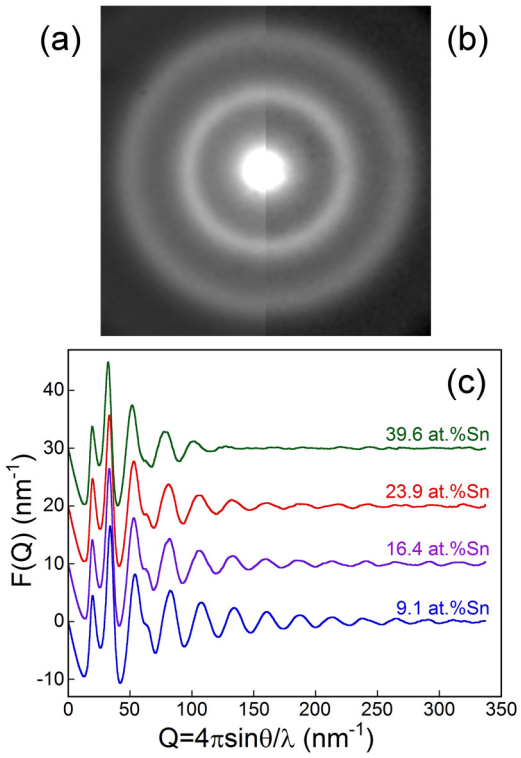

FIG. 1. Selected-area electron diffraction patterns of amorphous GeSn with (a) 9.1 and (b) 39.6 at. % Sn. (c) The diameter of the second halo ring in (a) is larger than that in (b). (c) Reduced interference functions, F(Q), of the as-sputtered GeSn with different Sn concentrations. For viewing clarity, the origin of each vertical axis was shifted by $10\ nm^{-1}$. A very weak intensity is detected up to the scattering vector of $\sim 320\ nm^{-1}$, but the amplitude of the peaks at the higher-scattering angle side rapidly damps with increasing Sn concentration.

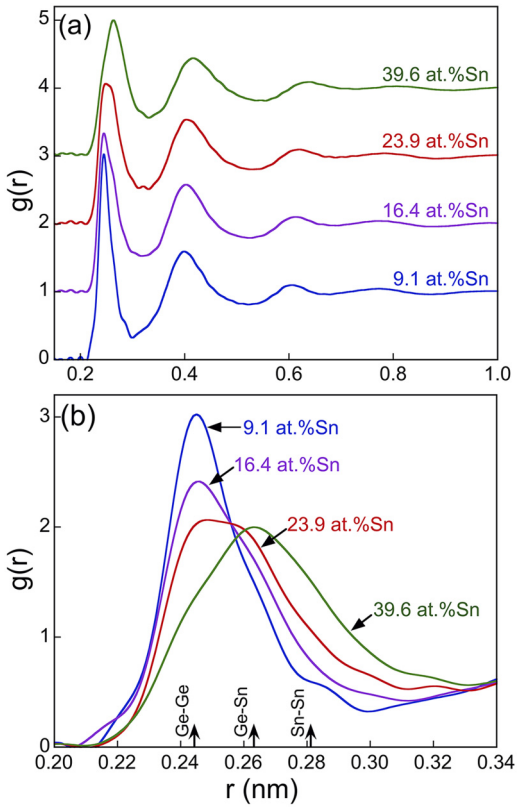

FIG. 2. (a) Atomic pair-distribution functions, g(r), obtained by Fourier transforming the F(Q) of Fig. 1(c). For viewing clarity, the origin of each vertical axis was shifted. (b) A magnified picture of the first peak in (a). Arrows on the abscissa denote the bond length of Ge-Ge (0.245 nm), Ge-Sn (0.263 nm), and Sn-Sn (0.281 nm) atomic pairs.

shows the existence probability of atoms as a function of a distance from the center of an arbitrary origin atom. Prominent first and second peaks appear at ~0.25 and ~0.40 nm, while the value of g(r) converges to unity at the longer distance side, indicating the lack of long-range order. There is no peak at ~0.47 nm corresponding to the third interatomic distance of the crystal with a diamond structure, reproducing the features of g(r) of group IV amorphous semiconductors.[30–35] It is apparent that the peak locations move to the longer distance side with increasing Sn concentration.

To obtain information on chemical short-range order within the first coordination shell, a magnified picture of the first peak in g(r) is shown in Fig. 2(b). The main peak of 9.1 at. % Sn specimens exists at 0.245 nm, which corresponds to the bond length of the Ge-Ge atomic pair. In addition to this main peak, a shoulder associated with the formation of the Ge-Sn atomic pair appears at ~0.26 nm in the specimen with 16.4 at. % Sn. This shoulder becomes more pronounced with increasing Sn concentration, and the main peak eventually shifts to 0.263 nm in the 39.6 at. % Sn specimen. This behavior is attributed to an increase of Ge-Sn and Sn-Sn atomic pairs within the first coordination shell. It should be noted that the g(r) around 0.30–0.32 nm becomes large with increasing Sn concentration. This is presumably due to the formation of β-Sn like metallic bonds (0.302 and 0.318 nm), in agreement with the rapid damping of the intensity profile with increasing Sn concentration [Fig. 1(c)].

B. Structural changes of amorphous GeSn on thermal annealing

We examined the effects of thermal annealing on amorphous structures using *in situ* TEM in combination with a heating holder. Figure 3(a) shows thermally-induced structural changes of amorphous GeSn. The annealing temperature is 230 °C for the 20.8 at. % Sn specimen and 200 °C for the 30.3 at. % Sn one. The former and the latter specimens crystallized at temperatures above and below the eutectic point (231 °C) of crystalline GeSn,[6] respectively, as described later. The specimen was annealed at elevated temperature for 10 min, and then the diffraction patterns were taken at room temperature: the specimens were repeatedly annealed between room and elevated temperatures. For comparison, the g(r) of the as-sputtered specimen is also shown. The second peak in the g(r) obtained from the amorphous GeSn with 20.8 at. % Sn is higher in 230 °C-annealed specimen (broken line) than in the as-sputtered one (solid line), while the height of the first peak is almost the same between these specimens. A similar behavior was also observed in structural relaxation of amorphous Si,[30] and, therefore, the changes in the g(r) of amorphous GeSn with 20.8 at. % Sn are attributed to structural relaxation. On the other hand, the peak height is almost the same between the as-sputtered and 200 °C-annealed amorphous GeSn with 30.3 at. % Sn. This suggests that the annealing temperature and time are not sufficient to induce remarkable structural relaxation.

Magnified pictures of the first peak are shown in Figs. 3(b) and 3(c). No remarkable change was observed in the peak position in the g(r) of the 20.8 at. % Sn specimen, as shown in Fig. 3(b). In contrast, the first peak of the 30.3 at. % Sn specimen moves to the shorter distance side by thermal annealing [Fig. 3(c)]. This is due to the fact that the number of atomic pairs with longer distance, i.e., Ge-Sn and Sn-Sn, decreases within the first coordination shell, as presumably phase decomposition occurs in amorphous GeSn prior to crystallization. We have recently examined the crystallization processes of amorphous GeSn under electron-beam irradiation and found that a weak halo ring due to Sn segregation appears in electron diffraction patterns of crystallized GeSn.[25] The critical concentration of Sn segregation under electron-induced crystallization was ~23 at. % Sn in the as-sputtered amorphous GeSn, which is in agreement with the present result.

C. Thermally-induced crystallization of amorphous GeSn

Figure 4(a) shows a selected-area electron diffraction pattern of the 20.8 at. % Sn specimen taken during annealing at 250 °C. Halo rings of the as-sputtered amorphous GeSn changed to Debye-Scherrer rings, indicating that an amorphous-to-crystalline phase transformation takes place at this temperature. The rings can be indexed from the inside as 111, 220, and 311 of a diamond structure, whereas no extra reflections due to a secondary phase exist in Fig. 4(a). Figure 4(b) shows the electron diffraction patterns taken at room temperature after cooling the specimen. This diffraction pattern is almost identical to Fig. 4(a), suggesting that Sn atoms are incorporated substitutionally into the Ge lattice.

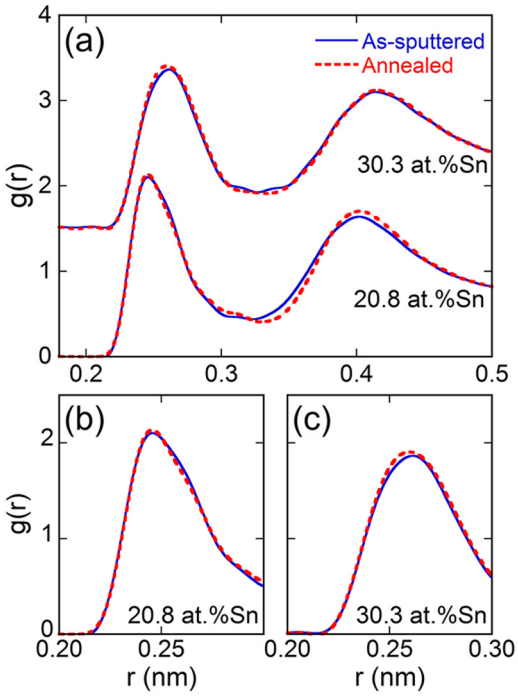

FIG. 3. (a) Atomic pair-distribution functions of amorphous GeSn before and after annealing: 20.8 at. % Sn (lower) and 30.3 at. % Sn (upper). The former and latter specimens were annealed at 230 °C and 200 °C, respectively. (b) and (c) Magnified pictures of the first peak in (a). The location of the first peak in (b) does not change before and after heat treatments, whereas it moves to the shorter distance side in (c) after thermal annealing.

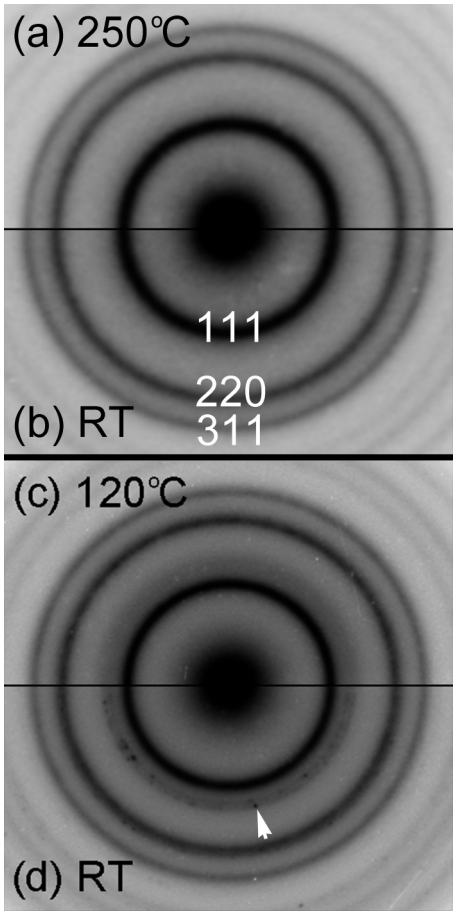

FIG. 4. Selected-area electron diffraction patterns of crystallized GeSn with [(a) and (b)] 20.8 and [(c) and (d)] 40.9 at. % Sn in an as-deposited state. To show the feature of the diffraction patterns clearly, the contrast is inversed. The specimens were annealed at (a) 250 and (c) 120 °C, and then cooled to [(b) and (d)] room temperature. Debye-Scherrer rings can be indexed from the inside as 111, 220, and 311 of a diamond structure, suggesting the substitutional incorporation of Sn atoms into Ge. No extra reflections associated with the secondary phase appear in (a) and (b). A halo ring is observed just outside the 111 ring at elevated temperature (c), while the Bragg spots due to β-Sn, marked with an arrow, appear after cooling (d).

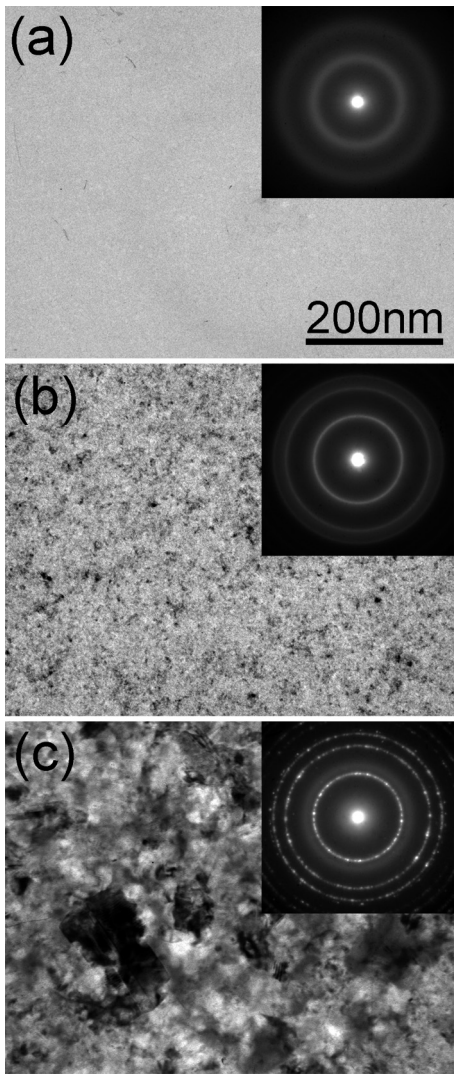

FIG. 5. A series of selected-area electron diffraction patterns and bright-field TEM images during thermal annealing of GeSn with 21.7 at. % Sn in the as-sputtered state. (a) 240, (b) 260, and (c) 300 °C. The amorphous structure is maintained at temperatures above the eutectic temperature (231 °C) in (a), while recrystallization occurs in (b). In addition to the coalescence of grains, the formation of molten Sn is detected in (c).

A diffraction pattern of the 40.9 at. % Sn specimen crystallized at 120 °C is shown in Fig. 4(c). In addition to the Debye-Scherrer rings due to a diamond structure, a new weak halo ring is observed just outside the 111 ring in Fig. 4(c). The appearance of the halo ring suggests that Sn ejected from the matrix is in a molten state despite the fact that the temperature (120 °C) is lower than the eutectic one (231 °C). Molten Sn presumably disperses in the nanoscale, and it is thought to induce a melting temperature depression. On the other hand, the Bragg spots corresponding to β-Sn appear at room temperature [Fig. 4(d)], indicating that the liquid-to-solid phase transformation of Sn occurs. Based on these results and radial distribution function analyses (Fig. 3), it is difficult to suppress Sn precipitates in GeSn with >25 at. % Sn obtained by our sample preparation techniques.

Here, the crystallization processes of GeSn with <25 at. % Sn were investigated in more detail. Figure 5 shows the structural evolution of GeSn with 21.7 at. % Sn during thermal annealing. The specimen was successively annealed. The diffraction pattern reveals halo rings, and no diffraction contrast is observed in the bright-field TEM image of Fig. 5(a) at 240 °C: GeSn maintains its amorphous structure above the eutectic temperature. On the other hand, the Debye-Scherrer rings appear in the diffraction pattern of the

specimen annealed at 260 °C, and diffraction contrast due to crystallites is observed in the bright-field image [Fig. 5(b)]. The continuous ring pattern transforms to the discontinuous spot pattern by further annealing [Fig. 5(c)], indicating the coalescence and growth of grains. Indeed, the corresponding bright-field image reveals the formation of the grains with a size of >100 nm. It should be noted that a weak halo ring is observed in the diffraction pattern of Fig. 5(c), indicating that Sn ejected from the matrix exists as a liquid. A similar behavior was also observed in the thermal crystallization of 16.4 at. % Sn specimen in our previous study.[26]

We evaluated the onset of crystallization of our specimens by *in situ* TEM. Crystallization of an amorphous material progresses via a nucleation and growth mechanism, and, therefore, the amorphous and recrystallized regions coexist. The crystallization temperature can be also determined by x-ray diffraction[2,15] and Raman spectroscopy,[2] but a certain volume of crystallites is required for their detection. TEM can directly observe the initial stage of crystallization at the atomic scale, and, therefore, the crystallization temperature obtained here is presumably lower than that determined by x-ray diffraction and Raman spectroscopy. Figure 6 shows the crystallization temperature as a function of Sn concentration. The temperature was continuously raised in increments of 20–50 °C, and the specimens were annealed at a certain temperature for 10 min. (The deviation of crystallization temperature between Figs. 3 and 6 originates from the difference of annealing sequence.) The crystallization temperature of amorphous Ge is 400–650 °C,[36] whereas amorphous GeSn crystallizes at lower temperature than this. It is apparent that the crystallization temperature decreases with increasing Sn concentration. In particular, the crystallization temperature of the specimens with >25 at. % Sn is lower than the eutectic temperature (231 °C). Toko *et al.*[12] succeeded in fabricating polycrystalline GeSn with 25 at. % Sn by subjecting a crystalline Sn/amorphous Ge bilayer film to heat treatment at 70 °C for 100 h. Our crystallization temperatures are higher than theirs because the heating time in the present experiment is as short as 10 min.

The temperature of Sn segregation is also plotted in Fig. 6. Sn atoms were partially ejected from the matrix and a small amount of molten Sn was formed at the initial stage of Sn segregation: the intensity of halo rings due to molten Sn was too weak to detect. To determine the temperature of Sn segregation, the specimens were repeatedly annealed from room temperature to elevated temperature after the crystallization. It is apparent that the Sn segregation occurs simultaneously with crystallization in the specimens with >25 at. % Sn. This result is reasonable, because the phase separation was already induced in the amorphous state of the specimens crystallized below the eutectic temperature (Fig. 3). On the other hand, the difference between crystallization and Sn segregation temperatures becomes large with decreasing Sn concentration. The Sn segregation temperature was also examined for crystalline GeSn grown epitaxially on a Ge/Si substrate.[37] As a result, it was found that the Sn segregation occurs at 350 °C in crystalline GeSn with 12 at. % Sn, which is much lower than that of amorphous GeSn with the same Sn concentration (480 °C). This suggests that the recrystallization of amorphous GeSn is an effective method to obtain solid solutions of GeSn.

D. Synthesis of large GeSn grains with high Sn concentration

Figure 7 shows the lattice parameter of crystallized GeSn as a function of annealing temperature. The legend denotes the initial Sn concentration of the amorphous state. The electron diffraction patterns were taken at room temperature after thermal annealing. Since the camera constant of TEM was calibrated by the Debye-Scherrer rings of polycrystalline thallium(I) chloride, the lattice parameter can be accurately determined in nanometer units up to the third decimal

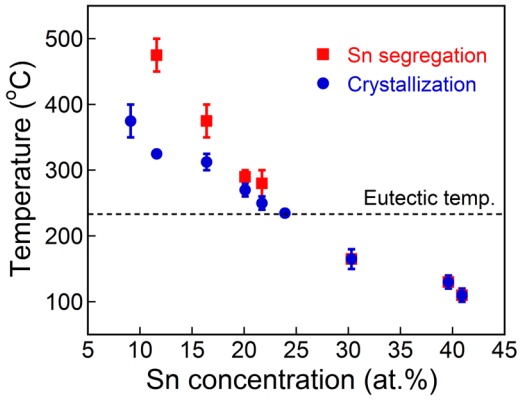

FIG. 6. Compositional dependence of crystallization (circle) and Sn segregation (square) of amorphous GeSn. The broken line denotes the eutectic temperature of the crystalline Ge-Sn binary system. The annealing temperature was successively raised, and the crystallization temperature was determined by the appearance of Debye-Scherrer rings in the diffraction pattern. On the other hand, the specimen was repeatedly annealed from room temperature to elevated temperature in order to detect the Sn segregation.

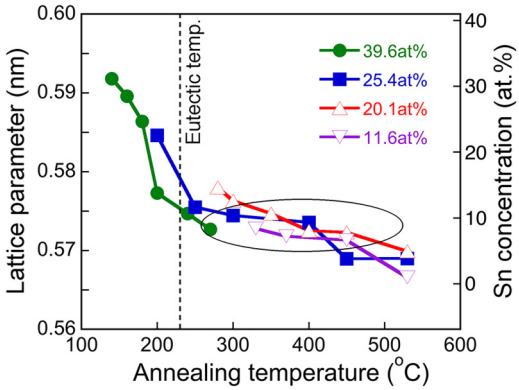

FIG. 7. Change of lattice parameter and Sn concentration with thermal annealing. The initial Sn concentration of amorphous GeSn is 11.6 (down-pointing triangles), 20.1 (triangles), 25.4 (squares), and 39.6 at. % (circles). Open and closed symbols denote the specimens crystallized above and below the eutectic temperature of crystalline GeSn, respectively. A temperature window where Sn segregation is suppressed exists in the encircled region.

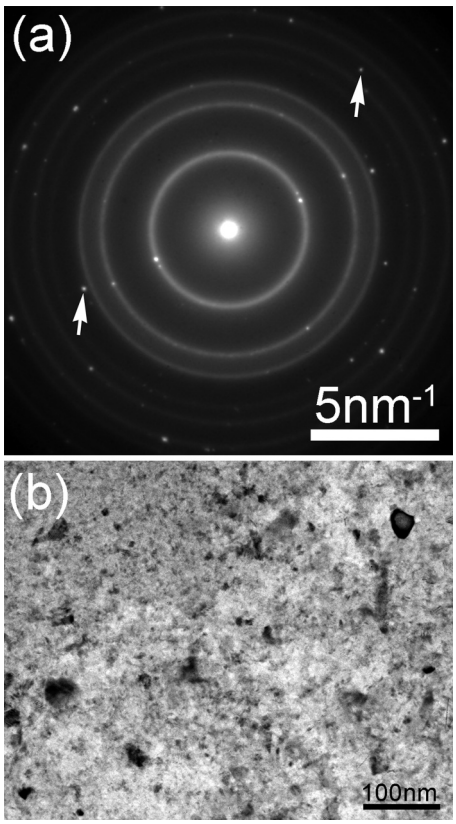

FIG. 8. (a) An electron diffraction pattern and (b) bright-field TEM image of GeSn with 12.0 at. % Sn annealed at 400 °C for 1 h. In addition to the Debye-Scherrer rings due to a diamond structure, sharp diffraction spots of GeSn crystallites are observed in (a). The reflections marked with arrows are caused by planar defects. The formed GeSn crystals have a size of 30–50 nm.

place. It is apparent that the lattice parameter of the specimens crystallized below the eutectic temperature rapidly decreases after crystallization, indicating that the ejection of Sn atoms from the Ge crystal progresses with thermal annealing. Although the lattice parameter of the 25.4 at. % Sn specimen greatly decreases just after crystallization, its reduction becomes small at temperatures ranging from 250 to 400 °C. The small reduction in the lattice parameter was also confirmed in a similar temperature range in GeSn with 11.6 and 20.1 at. % Sn that crystallize above the eutectic temperature.

From the lattice parameter, the Sn concentration was roughly estimated on the basis of Vegard's law. The lattice parameter was assumed to be 0.5658 nm for Ge and 0.6493 nm for α-Sn. Although the Sn concentration estimated here includes some errors because of the deviation from Vegard's law,[38] it was confirmed that our crystallized GeSn thin films possess a Sn concentration beyond the solubility limit of the bulk Ge-Sn binary system. Little Sn precipitation occurs just after crystallization. However, the Sn concentration estimated from the lattice constant is lower than that of the as-sputtered amorphous GeSn (see samples #19–22 in Table I), as observed previously.[25] Based on this result, it is considered that the Ge matrix contains at least the Sn concentration estimated from the lattice parameter. It should be noted that the change of Sn concentration with temperature becomes small at the temperature range circled in Fig. 7. This suggests that there is a temperature window where Sn segregation is suppressed.

A large amount of Sn atoms is substitutionally incorporated into Ge with a diamond structure. However, the grain size of GeSn crystallites was several nanometers just after crystallization [Fig. 5(b)]: there is a possibility that the performance of GeSn will be compromised. Takeuchi *et al.*[39] reported that a high carrier mobility can be realized in a polycrystalline $Ge_{0.98}Sn_{0.02}$ film with a grain size of 20–30 nm. We tried to increase the grain size by tuning the annealing conditions. A GeSn thin film with 12.0 at. % Sn in the initial amorphous state was annealed at a temperature window according to Fig. 6, i.e., 400 °C, for 1 h. The resultant diffraction pattern is shown in Fig. 8(a). Sharp Bragg spots appear in the diffraction pattern, and they are overlapped with the Debye-Scherrer rings. From the lattice parameter [0.574(2) nm: the last digit contains an error], the Sn concentration was estimated to be ∼10 at. %.

Some of the spots indicated by arrows do not overlap the Debye-Scherrer rings. Similar spots were also observed in pure Ge crystallized by electron-beam irradiation,[40] and, therefore, the extra reflections are not caused by Sn precipitates. We have recently found that they can be interpreted by considering planar defects, such as twins and stacking faults.[41] On a closer examination, some spots due to β-Sn are observed just outside the 111 ring. However, they are very few and their intensities are very weak, implying Sn segregation is highly suppressed. The bright-field TEM image corresponding to the diffraction pattern reveals the formation of GeSn grains with sizes of 30–50 nm [Fig. 8(b)].

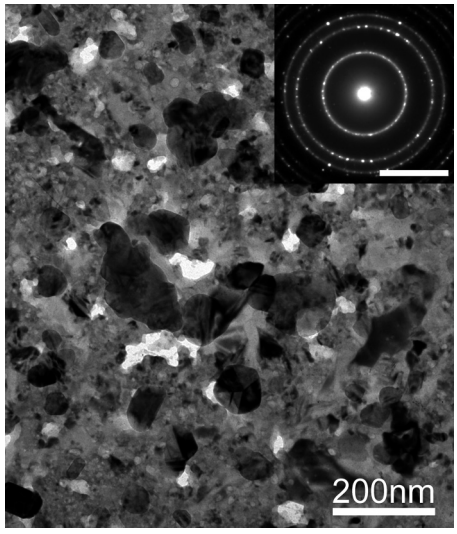

FIG. 9. (a) An electron diffraction pattern and (b) bright-field TEM image of GeSn with 6.3 at. % Sn annealed at 400 °C for 2 h. The diffraction pattern reveals discontinuous rings due to a diamond structure. It is apparent that GeSn crystals with a size of ∼200 nm are formed. The scale bar in the diffraction pattern corresponds to $1/d = 5\ nm^{-1}$.

Figure 9 shows another example of the fabrication of large GeSn grains with high Sn concentration. An amorphous GeSn thin film with 6.3 at. Sn% was annealed at 400 °C for 2 h. The Bragg spots of Sn in the diffraction pattern are very weak, indicating that Sn precipitation is highly suppressed. Discontinuous rings due to a diamond structure reveal the coalescence and growth of GeSn grains. The lattice parameter was estimated to be 0.570(5) nm, which corresponds to a Sn concentration of ~6 at. %. The corresponding bright-field image reveals the formation of GeSn grains with a size of ~200 nm. The results of Figs. 8 and 9 suggest that large GeSn grains with high Sn concentration can be formed by using the temperature window as in Fig. 6.

IV. CONCLUSIONS

Amorphous structures and thermally-induced structural changes of GeSn thin films prepared by sputtering were examined by TEM. Radial distribution function analysis revealed that the Ge and Sn atoms are mixed within the first coordination shell and no remarkable phase separation was detected in the as-sputtered amorphous GeSn. Prior to crystallization, structural relaxation occurred in amorphous GeSn with <25 at. % Sn during thermal annealing. On the other hand, Sn segregation in the amorphous matrix was detected in the specimens with >25 at. % Sn. Crystallization temperature decreased with increasing Sn concentration, and amorphous GeSn eventually crystallized at temperatures lower than the eutectic temperature of the Ge-Sn binary system when the Sn concentration was beyond ~25 at. %. In the GeSn thin films with >25 at. % Sn, Sn precipitated simultaneously with crystallization. On the other hand, the Sn precipitation temperature was higher than the crystallization temperature in the specimens with <25 at. % Sn, and the temperature difference became large with decreasing Sn concentration: a temperature window for suppressing the Sn segregation exists. Large GeSn grains with high Sn concentration were successfully formed by thermal annealing within the temperature window.

ACKNOWLEDGMENTS

We are grateful to Toshiki Kimura and Kohei Inenaga for their contributions to TEM observations. This work was partially supported by JSPS KAKENHI under Grant No. 16H04518.

REFERENCES

[1]S. Zaima, O. Nakatsuka, N. Taoka, M. Kurosawa, W. Takeuchi, and M. Sakashita, Sci. Technol. Adv. Mater. **16**, 043502 (2015).
[2]M. Uchida, T. Maeda, R. R. Lieten, S. Okajima, Y. Ohishi, R. Takase, M. Ishimaru, and J.-P. Locquet, Appl. Phys. Lett. **107**, 232105 (2015).
[3]K. Alberi, J. Blacksberg, L. D. Bell, S. Nikzad, K. M. Yu, O. D. Dubon, and W. Walukiewicz, Phys. Rev. B **77**, 073202 (2008).
[4]R. Chen, H. Lin, Y. Huo, C. Hitzman, T. I. Kamins, and J. S. Harris, Appl. Phys. Lett. **99**, 181125 (2011).
[5]W. Du, S. A. Ghetmiri, B. R. Conley, A. Mosleh, A. Nazzal, R. A. Soref, G. Sun, J. Tolle, J. Margetis, H. A. Naseem, and S.-Q. Yu, Appl. Phys. Lett. **105**, 051104 (2014).
[6]M. Hansen and K. Anderko, *Constitution of Binary Alloys* (McGraw-Hill, New York, 1958).
[7]M. Bauer, J. Taraci, J. Tolle, A. V. G. Chizmeshy, S. Zollner, D. J. Smith, J. Menendez, C. Hu, and J. Kouvetakis, Appl. Phys. Lett. **81**, 2992 (2002).
[8]M. Nakamura, Y. Shimura, S. Takeuchi, O. Nakatsuka, and S. Zaima, Thin Solid Films **520**, 3201 (2012).
[9]Y. Yoshizawa, S. Oguma, and K. Yamauchi, J. Appl. Phys. **64**, 6044 (1988).
[10]M. Kurosawa, N. Taoka, M. Sakashita, O. Nakatsuka, M. Miyao, and S. Zaima, Appl. Phys. Lett. **103**, 101904 (2013).
[11]R. R. Lieten, J. W. Seo, S. Decoster, A. Vantomme, S. Peters, K. C. Bustillo, E. E. Haller, M. Menghini, and J.-P. Locquet, Appl. Phys. Lett. **102**, 052106 (2013).
[12]K. Toko, N. Oya, N. Saitoh, N. Yoshizawa, and T. Suemasu, Appl. Phys. Lett. **106**, 082109 (2015).
[13]R. Matsumura, H. Chikita, Y. Kai, T. Sadoh, H. Ikenoue, and M. Miyao, Appl. Phys. Lett. **107**, 262106 (2015).
[14]M. Kim, W. Fan, J.-H. Seo, N. Cho, S.-C. Liu, D. Geng, Y. Liu, S. Gong, X. Wang, W. Zhou, and Z. Ma, Appl. Phys. Express **8**, 061301 (2015).
[15]R. Takase, M. Ishimaru, N. Uchida, T. Maeda, K. Sato, R. R. Lieten, and J.-P. Locquet, J. Appl. Phys. **120**, 245304 (2016).
[16]M. Kurosawa, N. Taoka, H. Ikenoue, O. Nakatsuka, and S. Zaima, Appl. Phys. Lett. **104**, 061901 (2014).
[17]H. Chikita, R. Matsumura, Y. Kai, T. Sadoh, and M. Miyao, Appl. Phys. Lett. **105**, 202112 (2014).
[18]M. Ishimaru, A. Hirata, M. Naito, I.-T. Bae, Y. Zhang, and W. J. Weber, J. Appl. Phys. **104**, 033503 (2008).
[19]Y. Hirotsu, M. Ishimaru, T. Ohkubo, T. Hanada, and M. Sugiyama, J. Electron Microsc. **50**, 435 (2001).
[20]M. Ishimaru, I.-T. Bae, Y. Hirotsu, S. Matsumura, and K. E. Sickafus, Phys. Rev. Lett. **89**, 055502 (2002).
[21]M. Naito, M. Ishimaru, Y. Hirotsu, and M. Takashima, J. Appl. Phys. **95**, 8130 (2004).
[22]M. Ishimaru, Nucl. Instrum. Methods Phys. Res. B **250**, 309 (2006).
[23]R. Nakamura, M. Ishimaru, H. Yasuda, and H. Nakajima, J. Appl. Phys. **113**, 064312 (2013).
[24]M. Ishimaru, I.-T. Bae, A. Hirata, Y. Hirotsu, J. A. Valdez, and K. E. Sickafus, Phys. Rev. B **72**, 024116 (2005).
[25]T. Kimura, M. Ishimaru, M. Okugawa, R. Nakamura, and H. Yasuda, Jpn. J. Appl. Phys. **56**, 100307 (2017).
[26]M. Higashiyama, M. Ishimaru, M. Okugawa, and R. Nakamura, in *Proceedings of Material Science and Technology 2018* (MS&T18, 2018), p. 284.
[27]T. Fukunaga, K. Itoh, T. Otomo, K. Moria, M. Sugiyama, H. Kato, M. Hasegawa, A. Hirata, Y. Hirotsu, and A. C. Hannon, Intermetallics **14**, 893 (2006).
[28]A. Hirata, Y. Hirotsu, K. Amiya, and A. Inoue, Phys. Rev. B **79**, 020205(R) (2009).
[29]A. Hirata, P. Guan, T. Fujita, Y. Hirotsu, A. Inoue, A. R. Yavari, T. Sakurai, and M. Chen, Nat. Mater. **10**, 28 (2011).
[30]K. Laaziri, S. Kycia, S. Roorda, M. Chicoine, J. L. Robertson, J. Wang, and S. C. Moss, Phys. Rev. B **60**, 13520 (1999).
[31]S. Kugler, G. Molnár, G. Petö, E. Zsoldos, L. Rosta, A. Menelle, and R. Bellissent, Phys. Rev. B **40**, 8030 (1989).
[32]J. Fortner and J. S. Lannin, Phys. Rev. B **39**, 5527 (1989).
[33]M. Ishimaru, S. Munetoh, and T. Motooka, Phys. Rev. B **56**, 15133 (1997).
[34]M. Ishimaru, M. Yamaguchi, and Y. Hirotsu, Phys. Rev. B **68**, 235207 (2003).
[35]K. Kohno and M. Ishimaru, Jpn. J. Appl. Phys. **57**, 095503 (2018).
[36]Z. H. Cao, P. Liu, X. K. Meng, S. C. Tang, and H. M. Lu, Appl. Phys. A **94**, 393 (2009).
[37]P. Zaumseil, Y. Hou, M. A. Schubert, N. von den Driesch, D. Stange, D. Rainko, M. Vigilio, D. Buca, and G. Capellini, APL Mater. **6**, 076108 (2018).
[38]A. V. G. Chizmeshya, M. R. Bauer, and J. Kouvetakis, Chem. Mater. **15**, 2511 (2003).
[39]W. Takeuchi, N. Taoka, M. Kurosawa, M. Sakashita, O. Nakatsuka, and S. Zaima, Appl. Phys. Lett. **107**, 022103 (2015).
[40]M. Okugawa, R. Nakamura, M. Ishimaru, H. Yasuda, and H. Numakura, J. Appl. Phys. **120**, 134308 (2016).
[41]M. Okugawa, R. Nakamura, A. Hirata, M. Ishimaru, H. Yasuda, and H. Numakura, J. Appl. Crystallogr. **51**, 1467 (2018).